JOC The Journal of Organic Chemistry

Article

pubs.acs.org/joc

Shifting the Energy Landscape of Multicomponent Reactions Using Aziridine Aldehyde Dimers: A Mechanistic Study

Lee Belding,[†] Serge Zaretsky,[‡] Benjamin H. Rotstein,[‡] Andrei K. Yudin,*[,‡] and Travis Dudding*[,†]

[†]Brock University, St. Catharines, Ontario L2S 3A1, Canada

[‡]Department of Chemistry, University of Toronto, Toronto, Ontario M5S 2J7, Canada

Supporting Information

ABSTRACT: A multicomponent reaction between an aziridine aldehyde dimer, isocyanide, and L-proline to afford a chiral piperazinone was studied to gain insight into the stereo-determining and rate-limiting steps of the reaction. The stereochemistry of the reaction was found to be determined by isocyanide addition, while the rate-limiting step was found to deviate from traditional isocyanide-based multicomponent reactions. A first-order rate dependence on aziridine aldehyde dimer and a zero-order rate dependence on all other reagents have been obtained. Computations at the MPWPW91/6-31G(d) level supported the experimental kinetic results and provide insight into the overall mechanism and the factors contributing to stereochemical induction. These factors are similar to traditional isocyanide-based multicomponent reactions, such as the Ugi reaction. The computations revealed that selective formation of a *Z*-iminium ion plays a key role in controlling the stereoselectivity of isocyanide addition, and the carboxylate group of L-proline mediates stereofacial addition. These conclusions are expected to be applicable to a wide range of reported stereoselective Ugi reactions and provide a basis for understanding the related macrocyclization of peptides with aziridine aldehydes.

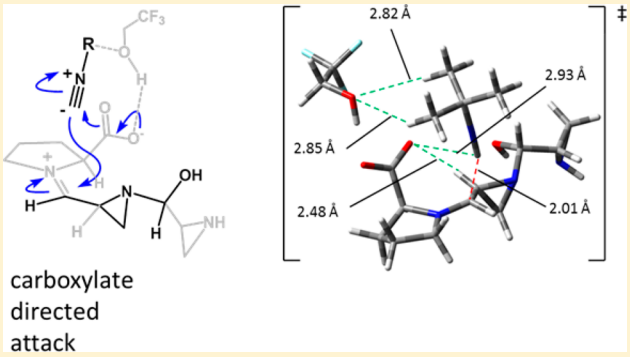

INTRODUCTION

Multicomponent reactions continue to attract attention in synthetic organic chemistry.[1] The combination of more than two reactants in a single process is an attractive means to construct diverse collections of small molecules.[2−4] The Ugi reaction links an amine, an aldehyde or ketone, a carboxylic acid, and an isocyanide to produce α-acylaminoamides. This four-component process has proven particularly useful in combinatorial chemistry[5,6] and natural product synthesis.[7−9] Computational studies by Fleurat-Lessard and co-workers have illuminated the mechanism of an Ugi reaction.[10] In both Ugi and Ugi−Smiles reactions, the isocyanide addition to form the isonitrilium ion was found to be irreversible, and Brønsted acid activation of the imine was found to accelerate an otherwise slow addition of isocyanide. Despite the frequent use of chiral components in diastereoselective Ugi reactions, a thorough understanding of the principles governing diastereoselectivity has not been achieved. As part of our ongoing efforts to deploy amphoteric molecules in chemical synthesis,[11,12] we applied aziridine aldehydes in the Ugi four-component condensation.[13] Of note was a structurally different outcome to what is to be expected of the Ugi process. Instead of nucleophilic attack by a solvent molecule on the mixed anhydride (i.e., solvolysis), the exocyclic aziridine attacks the mixed anhydride intermediate to form an aziridine amide in the final cyclic product. Using this chemistry, peptide macrocycles have been formed in a range of sizes and applied as biological probes for integrin receptors[14] and as solvatochromic mitochondria-penetrating probes.[15] A notable advantage over conventional cyclization is the opportunity to install additional functionality via the isocyanide component during the macrocyclization. Cycle-tail motifs, accessible via thioester isocyanides,[16] and cell-permeable bicyclic motifs have been reported.[17] Certain aspects of the aziridine aldehyde macrocyclization such as the absence of cyclodimerization and oligomerization can be linked to the innate charged-end attraction that is exhibited by the aziridine aldehyde based macrocyclization of peptides.[18] This property has served to inspire new forms of macrocyclization techniques.[19] Critically, the aziridine aldehyde cyclization also displays high diastereoselectivity of the isocyanide attack, which is seldom observed under Ugi conditions and merits an explanation. We report herein a combined experimental and computational study of the diastereoselective Ugi reaction with aziridine aldehyde dimers to afford piperazinones. Our work highlights the elements of control that emerge when dimeric aziridine aldehydes are made to react with α-amino acids and isocyanides and pave the way for in-depth investigation of the aziridine aldehyde macrocyclization process with peptides.

Received: June 3, 2014
Published: September 15, 2014

RESULTS AND DISCUSSION

When aziridine aldehyde dimer (*R*)-**1** was exposed to L-proline and *tert*-butyl isocyanide, cyclic piperazinone **4** was obtained in high yield (Scheme 1). (Aziridine aldehyde dimers with (*S*)-

Scheme 1. Three-Component Reaction of Aziridine Aldehyde with Isocyanide and L-Proline To Form Chiral Piperazinone 4[a]

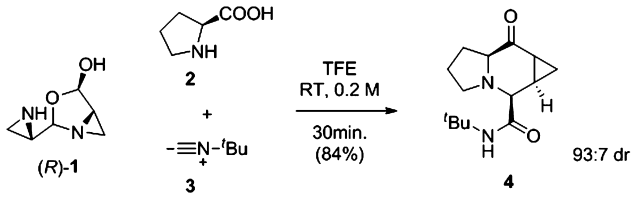

[a]Isolated yield reported for major product.

stereochemistry at the aziridine methine dimerize to form (*R*)-**1** dimers with (*R*)-stereochemistry at the hemiaminal and hemiacetal position.) While the reaction was initially projected to undergo iminium ion formation, isocyanide addition, and carboxylate attack, solvolysis of the mixed anhydride was interrupted by attack from the exocyclic nucleophilic aziridine. The relatively high molarity of this process (~0.2 M) and diastereoselectivity led us to study the role of aziridine aldehyde dimers in the interrupted process.

To gain insight into the nature of the rate-limiting step, we resorted to monitoring the product concentration by internally standardized LC/MS. Using single-ion-monitoring mode, the concentration of piperazinone product **4** was calibrated to the concentration of the internal standard, benzamide. This method facilitated a quantitative assessment of product formation during the course of the reaction (see the Supporting Information). Under pseudo-first-order conditions, the reaction was found to be first order in aziridine aldehyde (*R*)-**1**. Subsequently, kinetic dependence on other reactants was elucidated by varying the starting concentration of isocyanide, **3**, and L-proline, **2**. In all cases, product formation was logarithmic and independent of the concentration of other reagents.

The LC/MS-based kinetics were confirmed independently by a ^{13}C NMR-based method. In brief, ^{13}C-labeled **2** (at the carboxylate) was exposed to analogous pseudo-first-order conditions in 10% TFE-d_3/TFE, and product formation was quantified by integrating the aziridine amide carbonyl at 188.0 ppm. No significant rate changes were observed when the concentrations of either the isocyanide or L-proline were varied (see the Supporting Information). Our kinetic study suggests that the rate-determining step involves conversion of aziridine aldehyde dimer (*R*)-**1** into the acyclic dimer **5** (Scheme 2).

To gain further insight into the effect of dimeric assemblies on the diastereoselectivity of the isocyanide attack, we turned to computational modeling of this system. Calculations were carried out at the MPWPW91/6-31G(d)[20]/IEFPCM (solvent = trifluoroethanol) level of theory, using natural bond orbital (NBO) analysis to identify stabilizing interactions (see the Supporting Information for details). Starting from the aziridine aldehyde dimer, (*R*)-**1**, the reactive open dimer, **5**, is accessed through a TFE mediated ring opening of the oxazolidinol (**TS-1**(*R*), Figure 1).[21] Overall, this process is endothermic (ΔG_{rxn} =

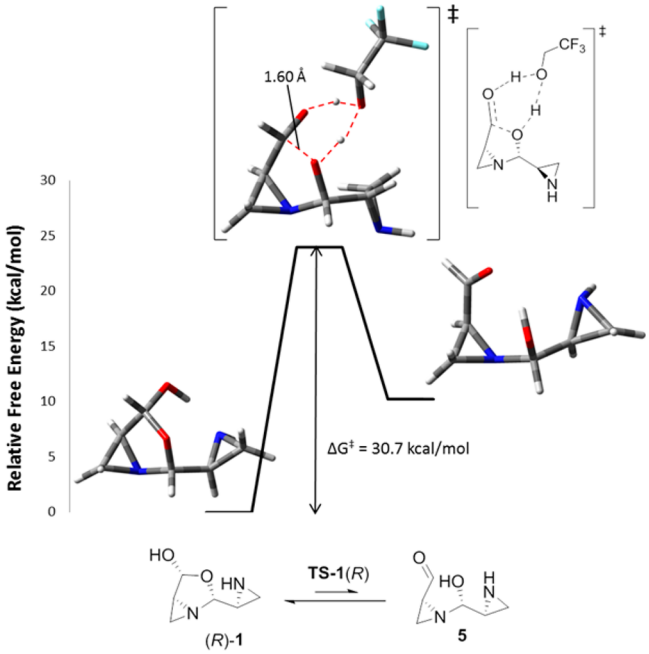

Figure 1. MPWPW91/6-31G(d)-computed structures and potential energy diagram for the formation of open dimer **5** from aziridine aldehyde dimer (*R*)-**1** through transition state **TS-1**(*R*).

Scheme 2. Proposed Condensation Mechanism for Aziridine Aldehyde Dimer Mediated Ugi Three-Component Reaction

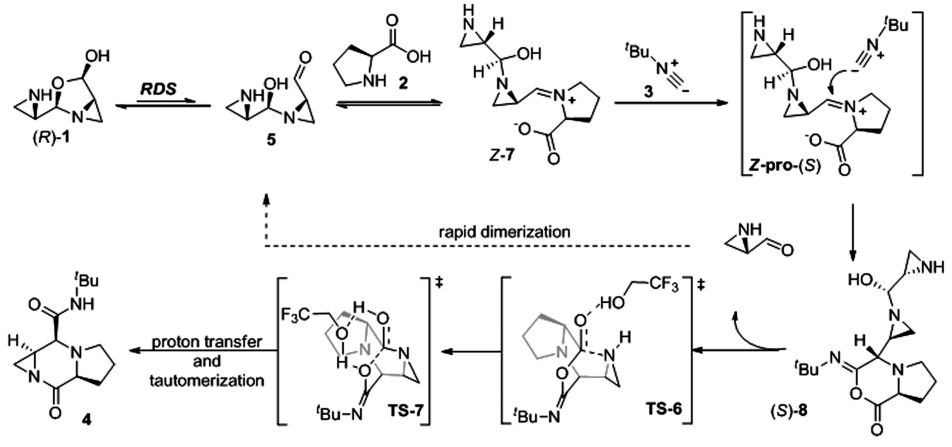

dx.doi.org/10.1021/jo501242r | J. Org. Chem. 2014, 79, 9465−9471

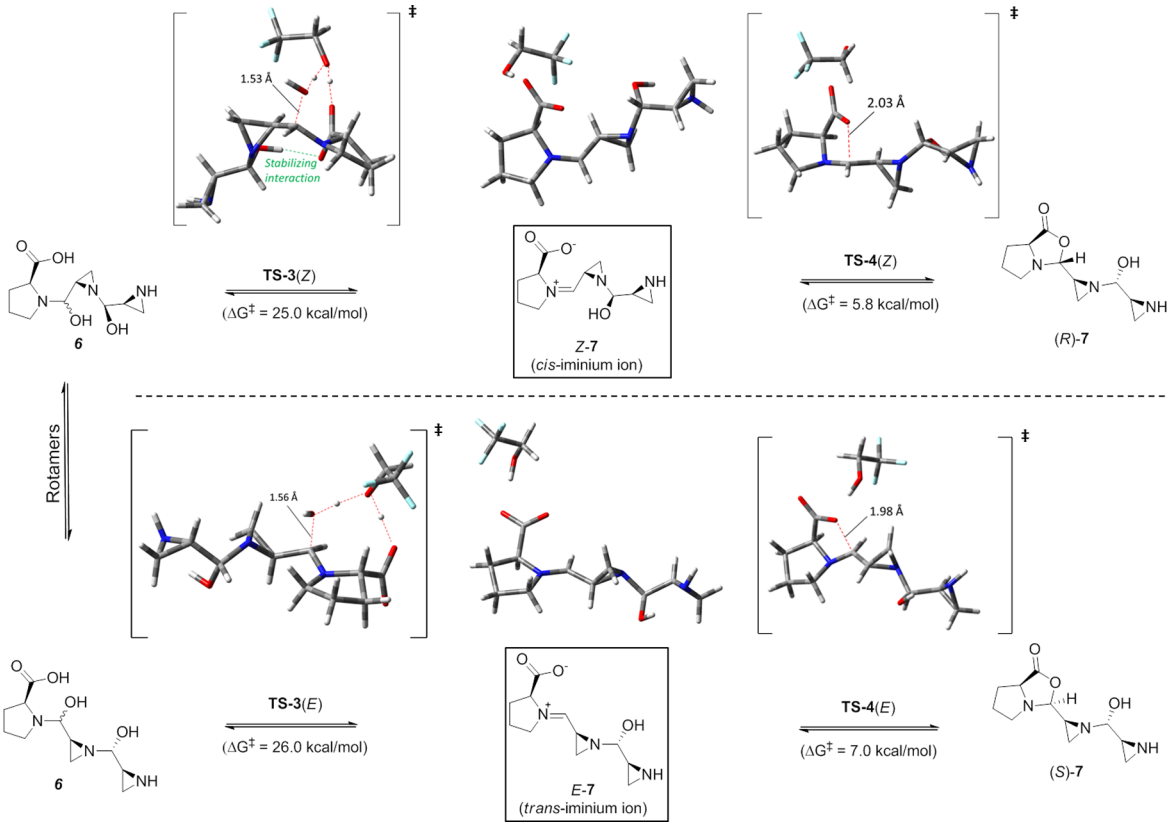

Figure 2. Dehydration transition states **TS-3**(*Z*) and **TS-3**(*E*) leading to iminium ions *Z*-**7** and *E*-**7** and their respective oxazolidinones (*R*)-**7** and (*S*)-**7**.

16.0 kcal/mol) with a significant activation barrier of 30.7 kcal/mol. Notably, reversion back to the starting oxazolidinol was selective for formation of (*R*)-**1** as the competing reaction to form the (*S*)-oxazolidinol had a 1.7 kcal/mol higher activation barrier (see the Supporting Information).

Proceeding from the open dimer **5**, condensation with L-proline (a two-step process involving **TS-2** and **TS-3**, see the Supporting Information) leads to formation of the iminium ion intermediates, *Z*-**7** and *E*-**7** (Figure 2), which are in equilibrium with the more thermodynamically stable oxazolidinones (*R*)-**7** and (*S*)-**7**, respectively, and interconvert by a low barrier process ($\Delta G^{\ddagger}$ = 5.8 and 7.0 kcal/mol). Key to this process is the divergent formation of either the *cis* or the *trans* iminium ion through dehydration via either **TS-3**(*Z*) or **TS-3**(*E*) (Figure 2), with the former being energetically favored by 1.0 kcal/mol. As a result, *Z*-iminium ion formation predominates. Leading to this energetic difference is the presence of a stabilizing interaction between the forming incipient carboxylate ion and the alcohol of the aziridine aldehyde in **TS-3**(*Z*).

Subsequent isocyanide addition to the iminium ion is stereodetermining, as is the case for most (if not, all) isocyanide-based multicomponent reactions. This process can occur through four possible modes of addition (Figure 2), ***E*-pro-(*R*)**, ***E*-pro-(*S*)**, ***Z*-pro-(*R*)**, and ***Z*-pro-(*S*)**, corresponding to attack on the *re*- or *si*-face of the *E*- or *Z*-iminium ion. Both the ***E*-pro-(*R*)** and ***Z*-pro-(*S*)** modes of addition result in isocyanide attack *cis* to the carboxylate group (i.e., *cis*-addition). In contrast, the ***E*-pro-(*S*)** and ***Z*-pro-(*R*)** modes of addition result in isocyanide attack from the opposite face of the iminium ion, *trans* to the carboxylate group (i.e., *trans*-addition).

To account for the role of solvent, the transition states were computed in the presence and absence of an explicit solvent molecule. Interestingly, in both cases and in contrast to previous assumptions,[22] *cis* isocyanide addition, occurring adjacent to the carboxylate group on the seemingly more sterically hindered face, was significantly favored. The basis for this counterintuitive finding can be attributed to carboxylate stabilization of the incoming nucleophile. At the transition state a molecule of TFE is activated by the carboxylate group and interacts with the incoming isocyanide, producing two stabilizing $C-H^{\delta+}\cdots O^{\delta-}$ interactions with the *tert*-butyl group (Figure 2), as evidenced by NBO analysis (E_{NBO} = 0.2 and 0.4 kcal/mol in ***Z*-pro-(*S*)**, and E_{NBO} = 0.7 and 1.1 kcal/mol in ***E*-pro-(*R*)**). Furthermore, the carboxylate group also stabilizes the transition state by means of a $C^{\delta+}\cdots O^{\delta-}$ interaction with the sp-hybridized isocyanide carbon (E_{NBO} = 1.7 kcal/mol in ***E*-pro-(*R*)** and 0.6 kcal/mol in ***Z*-pro-(*S*)**). Thus, it would appear that isocyanide addition is guided by stabilizing interactions between the carboxylate group and the isocyanide.

Although the ***Z*-pro-(*S*)** transition state is energetically favored over ***E*-pro-(*R*)**, it is important to note that they are not in direct competition because their iminium ion precursors are not readily interconvertible. (It is noteworthy that if iminium ion formation were reversible, the ***Z*-pro-(*S*)** addition mode is still energetically favored over the ***E*-pro-(*R*)** addition mode, and the reaction pathway remains, for all intents and purposes, unchanged.) Furthermore, once the iminium ion is formed, *cis*-addition mode is highly favored. As a result, the observed diastereoelectvity arises from preferential formation of the *Z*-iminium ion followed by an energetic preference for *cis* isocyanide addition.

dx.doi.org/10.1021/jo501242r | J. Org. Chem. 2014, 79, 9465−9471

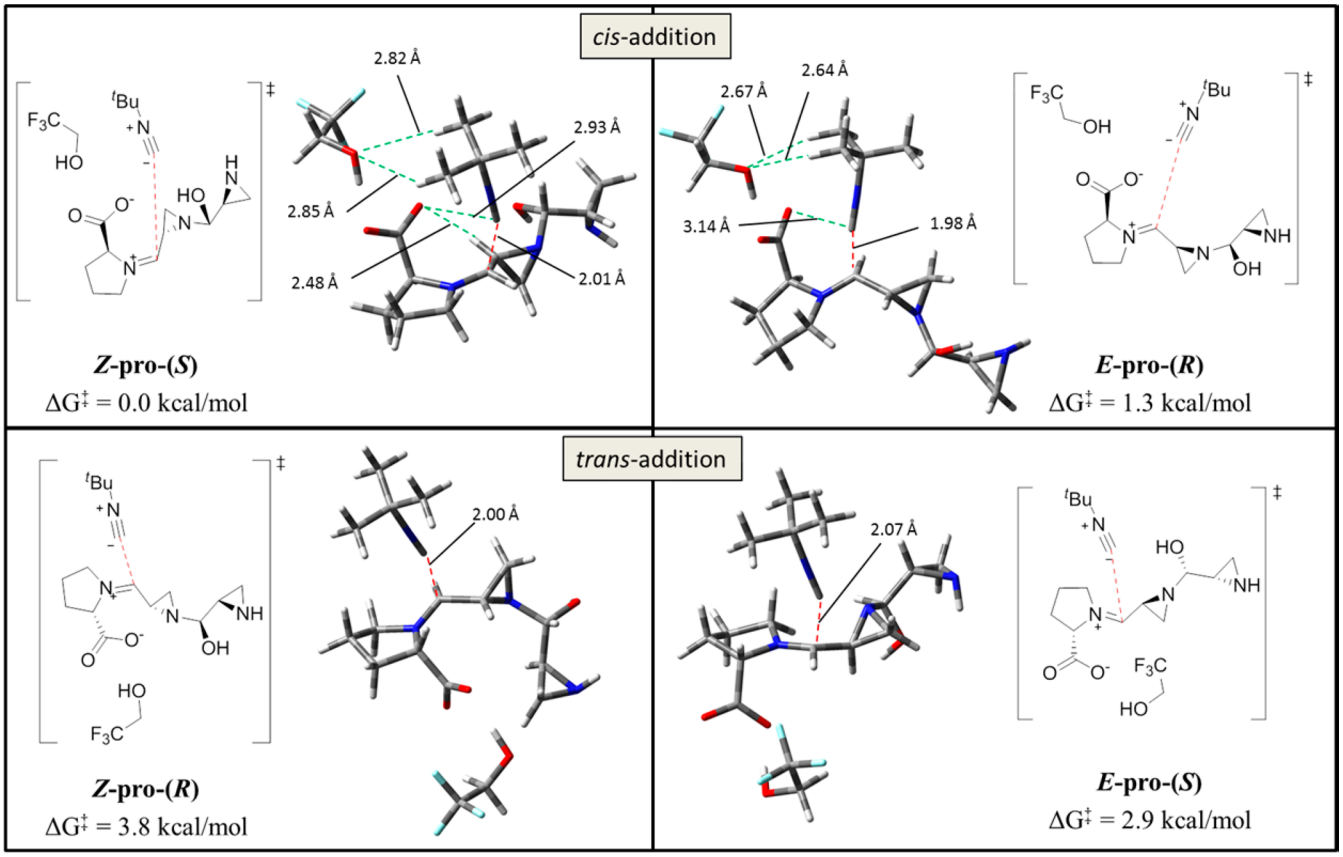

Figure 3. MPWPW91/6-31G(d)-computed isocyanide addition transition-state structures and relative free energies for ***E*-pro-(*R*)**, ***E*-pro-(*S*)**, ***Z*-pro-(*R*)**, and ***Z*-pro-(*S*)**.

Salient metrics of the lowest energy transition state, ***Z*-pro-(*S*)**, include a C···C bond-forming distance of 2.01 Å, a Bürgi-Dunitz attack trajectory[23] ($\phi_{(C-C-N)}$ = 107.3°), and the presence of a C−$H^{\delta+}$···$O^{\delta-}$ interaction between the carboxylate oxygen and the aziridine methine C−H (Figure 2, E_{NBO} = 1.1 kcal/mol). It is also noteworthy that the aziridine ring adjacent to the iminium ion is aligned in an s-*trans* conformation which allows for delocalization of electron density in the incipient C−C bond into the antiperiplanar C−C σ*-bond of the aziridine through negative hyperconjugation.[24] Of additional interest was the calculated HOMO for isocyanide addition (Figure 3). The HOMO of ***Z*-pro-(*S*)** exhibited no orbital density at the electron-deficient C−C bond-forming reaction site, indicative of an early transition state. This is also in line with previous findings by Cieplak on nucleophilic additions to carbonyls.[25] As such, the application of Cieplak's model was investigated further, which revealed that the transition state was stabilized by hyperconjugation from an antiperiplanar aziridine σ-bond C−C into the σ*-orbital of the incipient C−C forming bond (E_{NBO} = 5.6 kcal/mol), also consistent with the Cieplak model.

Taken together, it appears that the aziridine ring system serves two important stereoelectronic roles with respect to the C−C bond-forming isocyanide addition, acting as both a donor and an acceptor. First, electron density is delocalized from the forming C−C bond into an antiperiplanar σ*-bond of the aziridine. Second, hyperconjugation from the same antiperiplanar aziridine σ-bond is donated into the σ*-orbital of the incipient C−C forming bond. This push−pull relationship originates in large part from the ambiphilic nature of isocyanides, which possess a divalent carbon and are thus often considered carbenes.[26]

Addition of the isocyanide is followed by attack of the carboxylate oxygen atom into the π-system of *tert*-butyl isocyanide. In the *cis*-addition modes, the carboxylate group is aligned with the π-system of isocyanide in such a way that the transition states for addition lead directly to intermediates (*S*)-**8** (Figure 4) and (*R*)-**8**. In contrast, in the less energetically favored *trans*-addition modes the isocyanide is remote from the carboxylate group, making it inaccessible for a concerted ring closure, leading to zwitterionic intermediates (see the

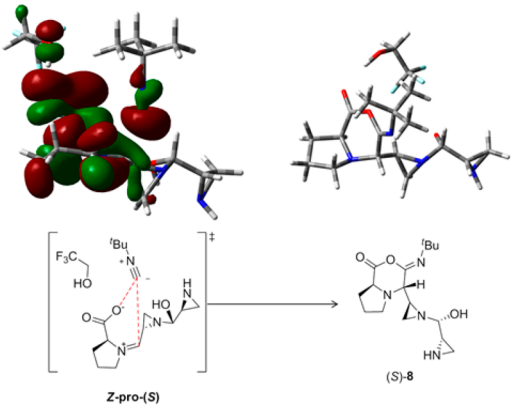

Figure 4. MPWPW91/6-31G(d)-calculated HOMO for the *cis*-addition transition state ***Z*-pro-(*S*)** and the computed product resulting from this transition state, (*S*)-**8**.

dx.doi.org/10.1021/jo501242r | J. Org. Chem. 2014, 79, 9465−9471

Supporting Information). Thus, the favored pathway is consistent with a concerted, asynchronous process. The resulting mixed anhydrides are highly thermodynamically favored, and the barriers to inversion are 27.9 kcal/mol for the (*S*)-product ((*S*)-**8**) and 27.7 kcal/mol for the (*R*)-product ((*R*)-**8**).

At that stage, protonation of the internal aziridine by TFE (intermediate (*S*)-**9**) facilitates the dissociation of an aziridine aldehyde monomer through **TS-5**(*S*) to yield intermediate (*S*)-**10** (Figure 5).

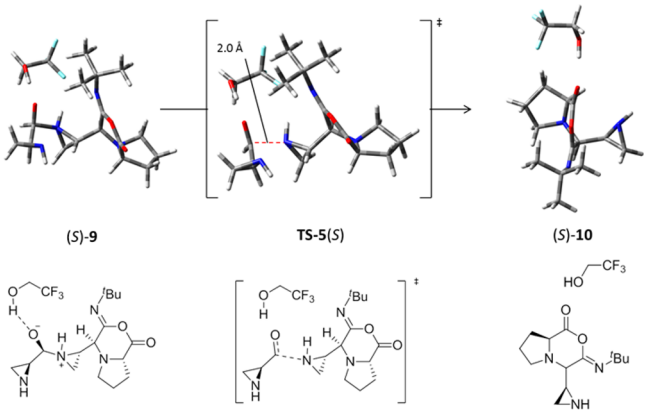

Figure 5. MPWPW91/6-31G(d)-computed structures of (*S*)-**9**, TS-**5**(*S*), and (*S*)-**10**.

Following dissociation, intramolecular attack of the free aziridine onto the carbonyl group of the mixed anhydride proceeds through TFE-mediated transition state **TS-6**(*S*), leading to a tetrahedral intermediate at the bridgehead of the two ring systems (intermediate (*S*)-**11**, Figure 6).

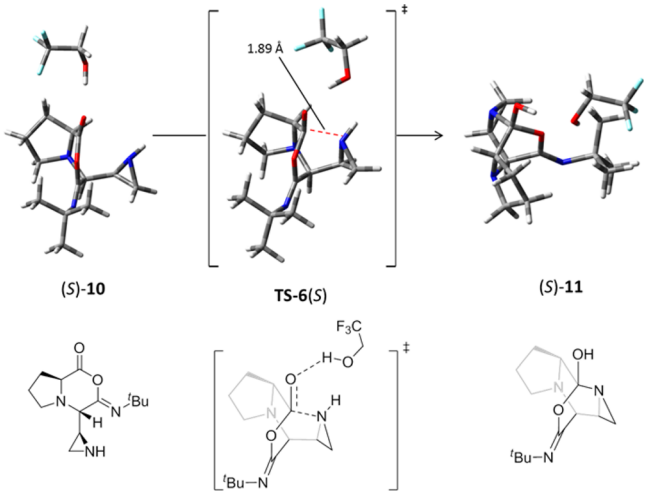

Figure 6. MPWPW91/6-31G(d)-computed structures of (*S*)-**9**, TS-**6**(*S*), and (*S*)-**10**. For simplicity, TFE was not included in the schematic for (*S*)-**9** and (*S*)-**10**.

This intermediate then undergoes a TFE-mediated proton transfer (**TS-7**(*S*), Figure 7) to reform the carbonyl group and cleave the ester linkage. The product iminol ((*S*)-**12**) then tautomerizes to the thermodynamically favored amide ((*S*)-**4**).

Taken together, the overall potential energy diagram for the reaction is depicted in Figure 8. In agreement with experimental results, opening the aziridine aldehyde dimer

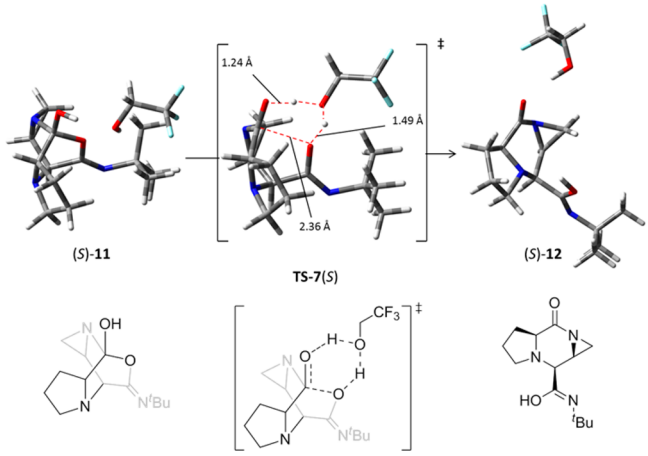

Figure 7. MPWPW91/6-31G(d)-computed structures of (*S*)-**11**, **TS-7**(*S*), and (*S*)-**12**. For simplicity, TFE was not included in the schematic for (*S*)-**11** and (*S*)-**12**.

(**TS-1**(*R*)) is rate limiting. The mechanism diverges into either the pro-(*R*) or pro-(*S*) pathway at **TS-3** as a result of the formation of either the *Z*- or *E*-iminium ion. At that stage, irreversible isocyanide addition sets the stereochemistry, forming intermediate **8**. Dissociation of an aziridine aldehyde monomer (**TS-5**) is followed by intramolecular transacylation of the aziridine nitrogen (via **TS-6** and **TS-7**) before eventually forming the product **4**.

CONCLUSION

To conclude, a multicomponent reaction between aziridine aldehyde dimer, isocyanide, and L-proline to afford chiral piperazinones was found to have a rate-limiting step that precedes isocyanide addition, which is in contrast to the majority of reported isocyanide-based multicomponent reactions. The reaction was found to have a first-order rate dependence on aziridine aldehyde dimer and a zero-order rate dependence on all other reagents. Computations at the MPWPW91/6-31G(d) level supported the experimental kinetics results and shed light on the overall mechanism, including the factors contributing to stereochemical induction. The computations revealed that selective iminium ion formation played an important role in stereochemical preference of isocyanide addition, and stereofacial selectivity was directed by the carboxylate group of L-proline. These findings will be instructive for understanding the related macrocyclization of peptides with aziridine aldehydes. Lastly, and perhaps most importantly, the concepts of the preferred imine or iminium ion intermediate arrangement and carboxylate position may be extrapolated to other reported stereoselective Ugi reactions in order to account for observed stereoselectivites.

EXPERIMENTAL SECTION

General Information. All solvents including TFE (2,2,2-trifluoroethanol) were of reagent grade quality. Products were characterized by ^{1}H and ^{13}C NMR spectroscopy and RP-HPLC/MS.

Chromatography. Flash column chromatography was carried out using 230−400 mesh silica gel. Thin-layer chromatography (TLC) was performed on precoated glass-backed TLC plates and visualized using a UV lamp (254 nm) and iodine stain.

Nuclear Magnetic Resonance Spectra. ^{1}H and ^{13}C NMR spectra were recorded on Varian Mercury 400 and Agilent 500 and 700 MHz spectrometers. ^{1}H NMR spectra were referenced to $CDCl_3$

dx.doi.org/10.1021/jo501242r | J. Org. Chem. 2014, 79, 9465−9471

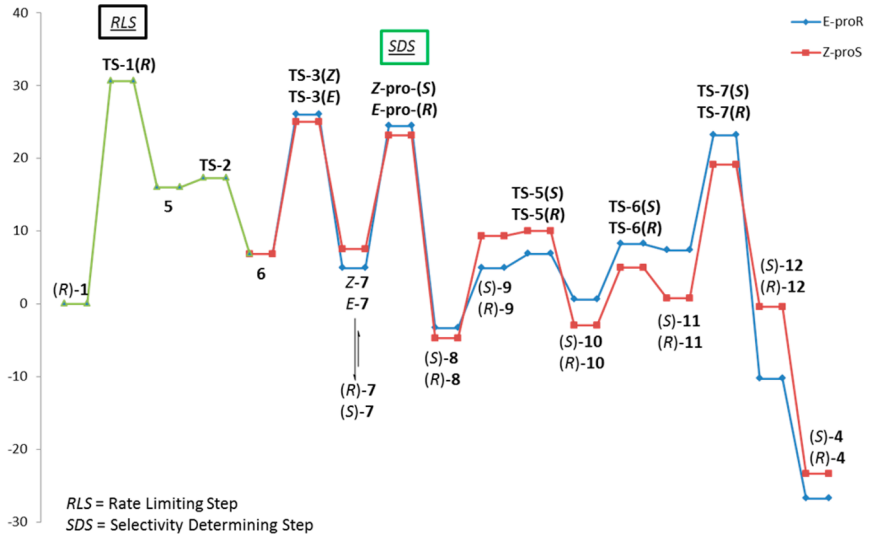

Figure 8. MPWPW91/6-31G(d)-computed reaction coordinate diagram for the formation of (*S*)-**4** and (*R*)-**4**.

(7.26 ppm) and CF_3CD_2OD (5.02 ppm), and ^{13}C NMR spectra were referenced to $CDCl_3$ (77.2 ppm) and CF_3CD_2OD (126.3 ppm). Peak multiplicities are designated by the following abbreviations: s, singlet; bs, broad singlet; d, doublet; t, triplet; q, quartet; m, multiplet; ds, doublet of singlets; dd, doublet of doublets; ddd, doublet of doublet of doublets; bt, broad triplet; td, triplet of doublets; tdd, triplet of doublets of doublets.

RP-HPLC/MS. Low-resolution mass spectra (ESI) were collected on an HPLC paired with a single-quad mass spectrometer. Compounds were resolved on an Agilent Poroshell 120 EC-C_{18}, 2.7 μm, 4.6 × 50 mm^2 column at room temperature with a flow of 1 mL/min. The gradient consisted of eluents A (0.1% formic acid in double distilled water) and B (0.1% formic acid in HPLC-grade acetonitrile). The gradient method started at 5% of B for the first 0.99 min, followed by a linear gradient from 5% to 95% B in 8.0 min. The column was then washed with 95% B for 1.0 min and equilibrated at 5% B for 1.5 min.

^{13}C NMR Kinetics Method. (*R*)-**1** was dissolved with 10% TFE-d_3/TFE (650 μL) and added to a 1 dram vial containing **2**. Then, **3** was pipetted into the vial, and the mixture was vortexed to make sure the reactants were as dissolved as much as possible. Afterward, the mixture was transferred to a 5 mm NMR probe and promptly put into the spectrometer. FIDs were collected on an Agilent 700 MHz equipped with a cold probe with a 30 s relaxation delay between single scans and no steady states. The ^{13}C peaks at 188.0 and 177.2 ppm, corresponding to the aziridine amide carbonyl for **4** and its TFE adduct, respectively, were integrated for their absolute values. NMRs were processed in Mnova 8.1.4 (Mestrelab Research) and data exported to Microsoft Excel.

HPLC–MS Calibration. Six samples were prepared of benzamide (0.05 M) in TFE with four concentrations of 0.05, 0.0375, 0.025, 0.0125, 0.0025, and 0.0005 M, respectively. Five microliter aliquots of the dilutions were pipetted into 500 μL of 2% TFE in HPLC-grade MeCN, and spectra were collected. Low-resolution mass spectra (ESI) were collected on an HPLC paired with a single-quad mass spectrometer. Compounds were resolved on an Agilent Poroshell 120 EC-C_{18}, 2.7 μm, 4.6 × 50 mm^2 column at room temperature with a flow of 1 mL/min. The gradient consisted of eluents A (0.1% formic acid in double distilled water) and B (0.1% formic acid in HPLC-grade acetonitrile). The gradient method started at 5% of B followed by a linear gradient to 67% B in 0.30 min and then a slower linear gradient to 75% in B by 3.00 min. The column was then washed with 95% B for 1.0 min and equilibrated at 5% B for 1.5 min. Single-ion monitoring (SIM) was used to detect the ions of **4** (*m*/*z* 252.2 and 352.2 for the TFE adduct) and benzamide (*m*/*z* 122.2). The MS detector was set to total ion count, SIM 122.2, SIM 252.2, and SIM 352.2, with Fast Scan enabled. The SIM spectra were integrated using the *Advanced Profile* in Chemstation (Agilent).

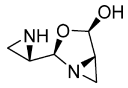

(2R,4R,5S)-2-((S)-Aziridin-2-yl)-3-oxa-1-azabicyclo[3.1.0]hexan-4-ol ((R)-1). Synthesized as per Rotstein, B. H.; Rai, V.; Hili, R.; Yudin, A. K. *Nat. Protoc.* **2010**, *5*, 1813–1822 and ref 11.

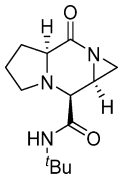

(3aS,8R,8aS)-N-tert-Butyl-3-oxooctahydroazirino[1,2-a]pyrrolo-[1,2-d]pyrazine-8-carboxamide (4). To a screw-cap vial equipped with a magnetic stirring bar was added L-proline (0.2 mmol) and 1 mL of TFE. (*R*)-**1** (0.1 mmol) and isocyanide (0.2 mmol) were then added sequentially, and the resulting mixture was stirred for 30 min (reaction was monitored by RP-HPLC/MS). The solvent was then evaporated under a stream of nitrogen. The mixture was then immediately purified by flash column chromatography (Hex → EtOAc) to yield 42 mg of the major product piperazinone product as a white solid in 84% yield. ^1H NMR ($CDCl_3$, 400 MHz) δ: 6.24 (bs, 1H), 3.42 (d, J = 6.2 Hz, 1H), 3.13 (dd, J = 9.5, 5.2 Hz, 1H), 3.05 (dd, J = 10.7, 4.6 Hz, 1H), 2.98 (t, J = 8.6 Hz, 1H), 2.41 (d, J = 4.8 Hz, 1H), 2.23 (d, J = 3.9 Hz, 1H), 2.21 (m, 1H), 2.13 (m, 2H), 1.86 (m, 2H), 1.35 (s, 9H) ppm. ^{13}C NMR ($CDCl_3$, 100 MHz) δ: 183.4, 169.0, 64.5, 63.2, 54.5, 51.4, 37.0, 30.5, 28.9, 22.0, 21.9 ppm. HRMS (ESI) calcd for $[C_{13}H_{21}N_3O_2 + H]^+$ calcd 252.1707, found 252.1712.

■ COMPUTATIONAL METHODS

Calculations were carried out at the MPWPW91/6-31G(d)[1] level of theory using the Gaussian 09[2] and GaussView v5.0.8 programs. To account for solvent effects, the integrated equation formalism polarized continuum solvation model (IEFPCM)[3] using solvent parameters for 2,2,2-trifluoroethanol was used throughout the computations, and explicit solvent molecules were included where necessary. All transition states were confirmed by the presence of a single imaginary frequency, and all minima were confirmed to be local minima by the presence of only real vibrational frequencies. Natural bond orbital (NBO) calculations were performed using Gaussian NBO version 3.1.[4]

dx.doi.org/10.1021/jo501242r | J. Org. Chem. 2014, 79, 9465–9471

■ ASSOCIATED CONTENT

Supporting Information

LC/MS and ^{13}C NMR-based kinetics data and coordinate and thermochemical data for all computed structures. This material is available free of charge via the Internet at http://pubs.acs.org.

■ AUTHOR INFORMATION

Corresponding Authors

*E-mail: ayudin@chem.utoronto.ca.

*E-mail: tdudding@brocku.ca.

Notes

The authors declare no competing financial interest.

■ ACKNOWLEDGMENTS

Financial support was provided in part by NSERC. L.B. is grateful for a NSERC CGS award, and S.Z. thanks OGS for financial support.

■ REFERENCES

(1) (a) Slobbe, P.; Ruijter, E.; Orru, R. V. A. *MedChemComm* **2012**, *3*, 1189−1218. (b) Rotstein, B. H.; Zaretsky, S.; Rai, V.; Yudin, A. K. *Chem. Rev.* **2014**, *114*, 8323−8359.

(2) *Isocyanide Chemistry: Applications in Synthesis and Material Science*; Nenajdenko, V. G., Ed.; Wiley-VCH: Weinheim, 2012.

(3) Dömling, A.; Ugi, I. *Angew. Chem., Int. Ed.* **2000**, *39*, 3168−3210.

(4) Ganem, B. *Acc. Chem. Res.* **2009**, *42*, 463−472.

(5) Hulme, C.; Dietrich, J. *Mol. Diversity* **2009**, *13*, 195−207.

(6) Banfi, L.; Bagno, A.; Basso, A.; De Santis, C.; Riva, R.; Rastrelli, F. *Eur. J. Org. Chem.* **2013**, *2013*, 5064−5075.

(7) Joullie, M. M.; Wang, P. C.; Semple, J. E. *J. Am. Chem. Soc.* **1980**, *102*, 887−889.

(8) Semple, J. E.; Wang, P. C.; Lysenko, Z.; Joullie, M. M. *J. Am. Chem. Soc.* **1980**, *102*, 7505−7510.

(9) Endo, A.; Yanagisawa, A.; Abe, M.; Tohma, S.; Kan, T.; Fukuyama, T. *J. Am. Chem. Soc.* **2002**, *124*, 6552−6554.

(10) Chéron, N.; Ramozzi, R.; El Kaïm, L.; Grimaud, L.; Fleurat-Lessard, P. *J. Org. Chem.* **2012**, *77*, 1361−1366.

(11) Hili, R.; Yudin, A. K. *J. Am. Chem. Soc.* **2006**, *128*, 14772−14773.

(12) Assem, N.; Hili, R.; He, Z.; Kasahara, T.; Inman, B. L.; Decker, S.; Yudin, A. K. *J. Org. Chem.* **2012**, *77*, 5613−5623.

(13) Hili, R.; Rai, V.; Yudin, A. K. *J. Am. Chem. Soc.* **2010**, *132*, 2889−2891.

(14) Roxin, Á.; Chen, J.; Scully, C. C. G.; Rotstein, B. H.; Yudin, A. K.; Zheng, G. *Bioconjugate Chem.* **2012**, *23*, 1387−1395.

(15) Rotstein, B. H.; Mourtada, R.; Kelley, S. O.; Yudin, A. K. *Chem.—Eur. J.* **2011**, *17*, 12257−12261.

(16) Rotstein, B. H.; Winternheimer, D. J.; Yin, L. M.; Deber, C. M.; Yudin, A. K. *Chem. Commun. (Cambridge)* **2012**, *48*, 3775−3777.

(17) Zaretsky, S.; Scully, C. C. G.; Lough, A. J.; Yudin, A. K. *Chem.—Eur. J.* **2013**, *19*, 17668−17672.

(18) Scully, C. C. G.; Rai, V.; Poda, G.; Zaretsky, S.; Burns, D. C.; Houliston, R. S.; Lou, T.; Yudin, A. K. *Chem.—Eur. J.* **2012**, *18*, 15612−15617.

(19) Londregan, A. T.; Farley, K. A.; Limberakis, C.; Mullins, P. B.; Piotrowski, D. W. *Org. Lett.* **2012**, *14*, 2890−2893.

(20) (a) Adamo, C.; Barone, V. *J. Chem. Phys.* **1998**, *108*, 664−675. (b) Perdew, J. P.; Chevary, J. A.; Vosko, S. H.; Jackson, K. A.; Pederson, M. R.; Singh, D. J.; Fiolhais, C. *Phys. Rev. B* **1992**, *46*, 6671−6687.

(21) For a related computational study on a solvent mediated ring-opening of a hemiacetal, see: Lewis, B. E.; Choytun, N.; Schramm, V. L.; Bennet, A. J. *J. Am. Chem. Soc.* **2006**, *128*, 5049−5058.

(22) Turner, C. D.; Ciufolini, M. A. *Org. Lett.* **2012**, *14*, 4970−4974.

(23) Bürgi, H. B.; Dunitz, J. D.; Lehn, J. M.; Wipff, G. *Tetrahedron* **1974**, *30*, 1563−1572.

(24) Tomoda, S. *Chem. Rev.* **1999**, *99*, 1243−1263.

(25) (a) Cieplak, A. S. *J. Am. Chem. Soc.* **1981**, *103*, 4540−4552. (b) Cieplak, A. S. *J. Org. Chem.* **1988**, *63*, 521−530. (c) Cieplak, A. S.; Tait, B. D.; Johnson, C. R. *J. Am. Chem. Soc.* **1989**, *111*, 8447−8462.

(26) Ramozzi, R.; Chéron, N.; Braïda, B.; Hiberty, P. C.; Fleurat-Lessard, P. *New J. Chem.* **2012**, *36*, 11137−1140.